Effects of small-scale features and local wind forcing on tracer dispersion and estimates of population connectivity in a regional scale circulation model

L. L. Rasmussen,[1] B. D. Cornuelle,[2] L. A. Levin,[1] J. L. Largier,[3] and E. Di Lorenzo[4]

[1] A small-scale model of the Southern California–Northern Baja California coastline has been developed to explore dispersion over the continental shelf, with specific attention to physical parameters pertinent to simulations of larval dispersal and population connectivity. The ROMS simulation employs a nested grid system, with an inner domain resolution of 600 m and an outer domain resolution of 1.5 km. Realistic bathymetry and forcing were employed to investigate the effects of passive transport of tracers introduced at locations with known communities of mytilid mussels along the coastline. The effects of topographic resolution, boundary conditions, and choice of meteorological forcing products on dispersion rates, tracer trajectories, and the subsequent measures of population connectivity were examined. In particular, the choice of wind forcing product resulted in different circulation patterns and tracer trajectories and had especially important consequences on measures of larval connectivity such as self-seeding, potential for larval settlement (import), and contribution to the pool of available larvae (export). While some forcing products performed better when model data were compared to field measurements, no product was clearly superior. The uncertainty in results, which may appear minor in larger-scale temperature or surface velocity fields, is significant when examining a sensitive passive tracer. This modeling uncertainty needs to be addressed when interpreting connectivity results.

Citation: Rasmussen, L. L., B. D. Cornuelle, L. A. Levin, J. L. Largier, and E. Di Lorenzo (2009), Effects of small-scale features and local wind forcing on tracer dispersion and estimates of population connectivity in a regional scale circulation model, *J. Geophys. Res.*, *114*, C01012, doi:10.1029/2008JC004777.

1. Introduction

[2] Numerical ocean circulation models are used increasingly in environmental and ecological applications, including assessing larval dispersal and connectivity, dispersion of point source pollutants, and transport of toxic or invasive species of marine life. Model simulations are often used because larvae are small and field sampling is constrained by the practicalities of cost, scale, and biological feasibility. When in situ methods such as chemical tracers, lagrangian drifters, and biological tagging are impractical because of high dilution rates, difficulty and expense of tracking, or the small size, large range, and complex life history of the organisms, models can provide a flexible alternative platform for experimentation.

[3] However numerical models also have many limitations. While large basin-scale and meso-scale circulation models have advanced rapidly over the last decades, modeling processes on small scales continues to be a challenge. Larval dispersion over large spatial and temporal scales may be studied with basin-scale or mesoscale numerical models [*Cowen et al.*, 2000; *Kettle and Haines*, 2006; *Paris et al.*, 2005] and genetic methods [*Galindo et al.*, 2006; *Palumbi*, 2003; *Hedgecock et al.*, 2007] but many of the problems in marine ecology, conservation, and environmental protection operate on regional scales or smaller. Examples include sustainability and connectivity of local populations [*Siegel et al.*, 2003; *James et al.*, 2002], propagation of invasive species [*Anderson et al.*, 2005; *Johnson et al.*, 2005], and health and ecological impacts of sewage outfalls and oil spills [*Signell et al.*, 2000; *Byers and Pringle*, 2006; *Largier*, 2003; *Hodgins et al.*, 1998; *Washburn et al.*, 1992]. For these applications, models must be able to simulate processes that are forced locally by small-scale variations in topography, wind fields, and source inputs. Models utilizing idealized topography or forcing have provided insight into specific processes, for example the effects of topographic features such as headlands or islands [*Signell and Geyer*, 1991; *Caldeira et al.*, 2005], frontal dynamics [*Scotti and Pineda*, 2007], and stochastic pro-

---

[1]Division of Integrative Oceanography, Scripps Institution of Oceanography, La Jolla, California, USA.
[2]Physical Oceanography Research Division, Scripps Institution of Oceanography, La Jolla, California, USA.
[3]Bodega Marine Laboratory, University of California, Davis, California, USA.
[4]School of Earth and Atmospheric Sciences, Georgia Institute of Technology, Atlanta, Georgia, USA.

cesses [*Mitarai et al.*, 2007]. However, while the physical variability and intermittency of the system has a large effect on both long- and short-term connectivity patterns, the products used to force small-scale models may introduce another significant source of uncertainty to results.

[4] The dependence of dispersion results on the interaction of small-scale bathymetric features, locally variable wind fields, and episodic events is still problematic [*Kinlan and Gaines*, 2003; *Werner et al.*, 2007]. Differences in eddy formation, meanders, and eddy kinetic energy have been shown to be related to coastline topography and model resolution [*Marchesiello et al.*, 2003]. In addition, the availability of high-resolution wind forcing data near the coast has been a long standing impediment to realistic simulations of inner shelf processes. [*Marchesiello et al.*, 2003] examined the California Current system in a 3.5 km resolution model and found significant differences in the structure of alongshore currents and countercurrents depending on the resolution of the wind product used. Similarly, *Capet et al.* [2004] found differences in nearshore wind speed drop off and wind stress curl between three resolutions of modeled winds that changed the strength and location of nearshore upwelling responses.

[5] Here we describe the development of a physical circulation model designed to investigate larval dispersion and connectivity along the Southern California/Northern Baja California coastline. This region is one of complex bottom topography, a weak and highly variable wind field, and significant effects from remote forcing [*Pringle and Riser*, 2003]. Located in the lee of Pt Conception and in the southeast quadrant of the Catalina Eddy, the wind field here is weaker than along the coast to the north and south and varies on a shorter temporal scale (hours to days). These features make simulation of tracer transport especially sensitive to model resolution, small-scale accuracy in forcing products, and bathymetry.

[6] Through the development of a small-scale (0.6−1.5 km) coastal model designed for inner-shelf dispersion and population connectivity applications, we address modeling issues of particular importance for processes with high variability over small spatial or temporal scales. We present an ensemble of results to highlight the impact of model forcing choices on biological questions. Our emphasis is on processes critical to regional larval dispersion problems, such as vertical structure of the water column and tracer dispersion patterns. These processes are found to be very sensitive to details of wind forcing, including the relative effects of local vs remote forcing, and are more sensitive to small variations and uncertainties than physical fields such as temperature. Wind forcing products for the inner shelf regions have been particularly problematic for small-scale circulation modeling, and we use a case-study to explore in depth the consequences of forcing choices on the interpretation of results for estimating larval transport and connectivity.

2. Model Formulation

[7] The Regional Ocean Modeling system (ROMS) is a free surface, terrain-following primitive equation ocean model [*Shchepetkin and McWilliams*, 2005; *Moore et al.*, 2004; *Song and Haidvogel*, 1994] capable of high-resolution descriptions of coastal and basin-wide flows. The use of ROMS is widespread in the oceanographic community and a variety of studies exist that investigate the dynamics of coastal ocean circulation [*She and Klinck*, 2000; *Di Lorenzo*, 2003; *Marchesiello et al.*, 2003; *Koné et al.*, 2005; *Di Lorenzo et al.*, 2005; *Warner et al.*, 2005; *Penven et al.*, 2006]. Development of various ROMS simulations with about 1 km resolution for coastal California (California Current, Southern California Bight) is ongoing and will provide a source for intercomparison of results and/or model data for nesting or boundary conditions [e.g., *Dong and McWilliams*, 2007].

2.1. Domain and Model Configuration

[8] The ROMS 3.0 simulation designed for this region consists of two 1-way nested model domains. The domain size was selected to enable larval connectivity experiments with simulated releases at actual spawning sites, and to provide ample room north and south of the sites to track tracer releases for a typical larval planktonic period of the mytilid mussel species under study, *M. californianus* and *M. galloprovincialis* (2−4 weeks). The outer domain size was also designed to extend far enough to include the stronger wind forcing south of 32N which can have a significant effect on local circulation in the San Diego area *Pringle and Riser* [2003]. Both model domains contain 30 terrain-following vertical layers, with highest resolution near the surface. The outer domain extends 150×300 km, with a resolution of 1.5 km, and the inner domain covers 65×150 km with 600 m resolution (Figure 1).

[9] The model region has an assortment of topographic features that all may affect final dispersion patterns, including headlands, steep submarine canyons, and offshore islands and seamounts. Compared to early simulations with more idealized coastline and bathymetry, inclusion of more realistic topography added small-scale features to the inner shelf circulation such as local retention zones and transport barriers which are critical to determining the fate of larvae or pollutants. The final bathymetry was created from a combination of ETOPO2 2-minute and NOAA 15-second data. The bathymetry has been smoothed to a maximum slope parameter r_{max} of 0.10. The slope parameter ($r = \Delta h / 2h_{mean}$) is a ratio of the maximum difference between adjacent grid cell depths and the mean depth at that point, used to assess the potential impact of errors induced by terrain-following (s-coordinate) horizontal layers. In regions with steep terrain combined with shallow depths, a relatively small r_{max} is necessary to prevent pressure gradient errors which result in artificial currents developing from a state of rest with no forcing [*Mellor et al.*, 1998; *Haney*, 1991; *Beckmann and Haidvogel*, 1993]. To estimate the magnitude of flow induced from pressure gradients caused by the terrain-following sigma layers, the model was run for 21 days with horizontally uniform stratification and no wind or heat flux forcing. We find that with $r \leq 0.10$, these residual velocities are small (2−3 cm/s) compared to the actual forced currents. *She and Klinck* [2000] were able to achieve error flows as small as 0.7 cm/s in a simulation of flow around a canyon, but the scale of the feature was much larger than those in this domain, and the equivalent r_{max} was approximately 0.05.

[10] The advection schemes employed by the simulation are third-order upwind horizontal and fourth-order centered
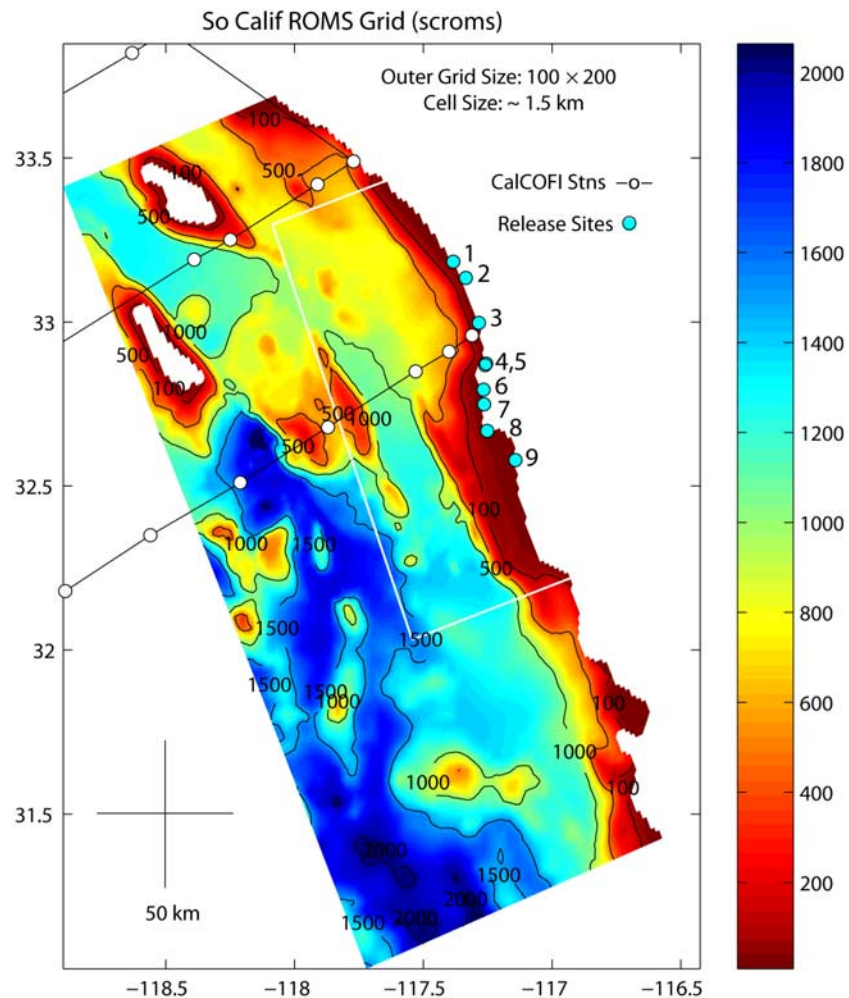
Figure 1. Domain and bathymetry for inner (600 m resolution) and outer (1.5 km resolution) grids. Blue dots indicate the modeled larval release sites, Site 1 at the north through Site 9 at the south. White dots are the CalCOFI CTD stations used to initialized the model.

vertical for temperature, salinity and passive tracers. Laplacian horizontal mixing is used for momentum, temperature, salinity and tracers. In addition, the Large/McWilliams/Doney interior mixing scheme is employed for mixing due to shear instability and the LMD local K-Profile Parameterization is applied at the surface boundary layer, and for nonlocal transport [*Large et al.*, 1994]. Input parameters are given in the Appendix.

[11] Coordinate systems for the model grid are oriented with u velocity in the cross-shelf direction (perpendicular to the long axis of the domain, positive shoreward) and v in the alongshore direction (parallel to the long axis, positive northward). Coordinates are not rotated for wind speed plots, but oceanographic orientation is used such that u is the westward component and v is the northward component.

2.2. Initialization and Boundary Conditions

[12] Initial conditions are taken from quarterly California Cooperative Oceanic Fisheries Investigation (CalCOFI) cruises (Scripps Institution of Oceanography, 2006). Because of the cross-shelf uniformity of the data on the transect in the center of the domain, a single profile from transect line 93 was selected as representative. T,S data from the cruise

nearest in time are applied to the domain according to depth and are uniform horizontally (for a similar approach see *Cervantes and Allen* [2006]). Surface heat flux forcing is from NCEP reanalysis daily climatic data. All simulation results shown are from models started on 1 May 2003 after prior spin up of 3–4 days. The time period was chosen to correspond to dates of population connectivity field experiments in this region utilizing trace elemental fingerprinting of juvenile mussels [*Becker et al.*, 2007].

[13] A number of experiments were run to test the effect of boundary conditions on the circulation within the inner domain. Figure 2 shows surface velocity for the inner domain run over the same time period with open versus closed boundaries. Both simulations are forced with a spatially uniform but temporally variable wind field. The model is spun up with the same wind field for 3–4 days, and the velocity fields shown are 21 days later. The open boundary simulation incorporates T, S, surface height, and velocity boundary conditions from a simultaneous run of the outer domain, forced with the same wind field. Including the velocity field from the outer domain as a boundary condition significantly changed the circulation pattern and the velocity magnitude in the inner domain. Subsurface and
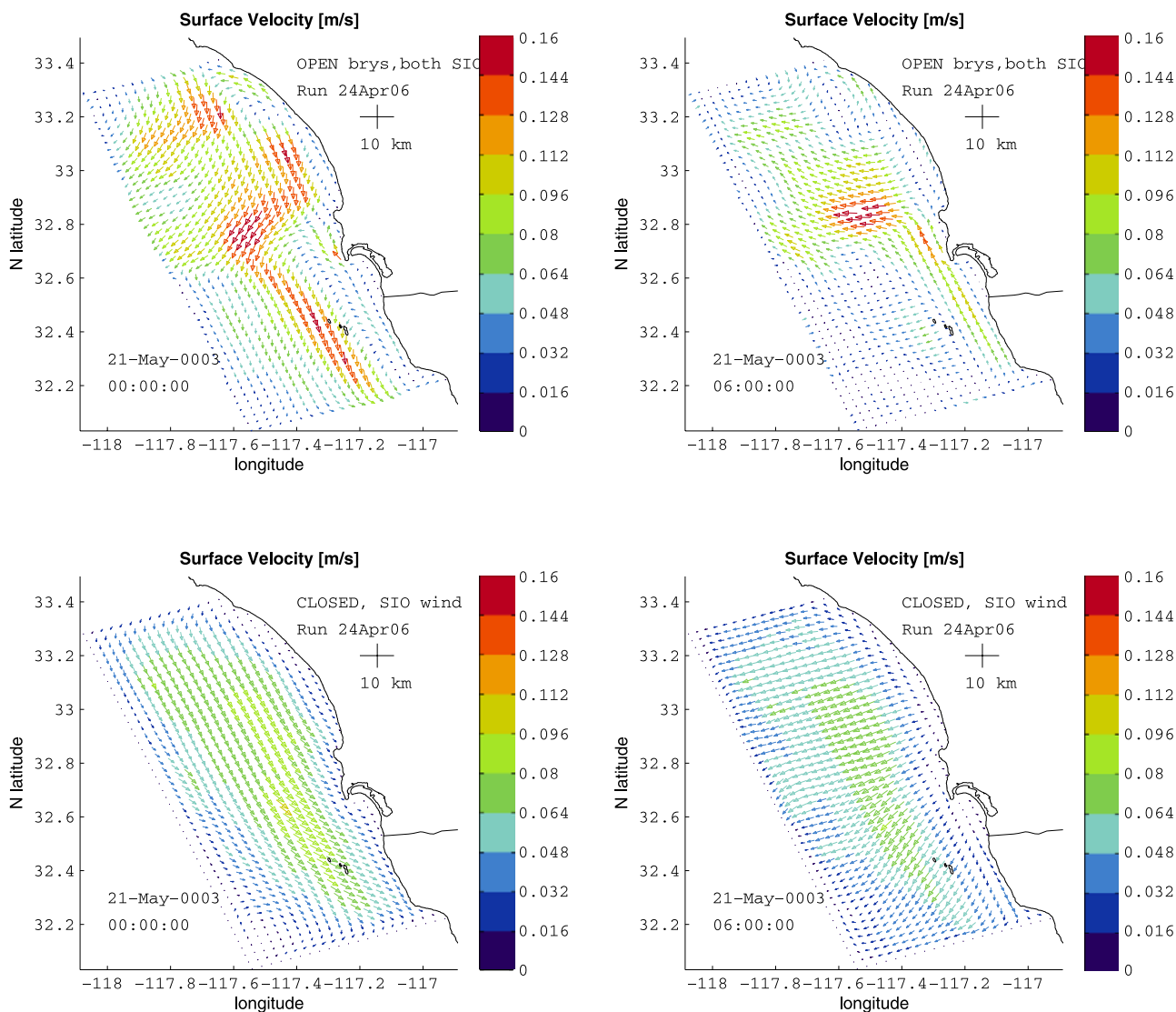
Figure 2. Surface velocity for inner model with open boundaries (top) and closed boundaries (bottom). Panels on left are at 00:00, right at 06:00. The open boundary case is run with local Scripps Pier winds on both inner and outer grids. Model is shown for 21 May 2003, 21 days after completion of spin up.

bottom velocities were also significantly impacted, and frequently velocities from open and closed boundary cases were in opposite alongshore directions. For small organisms with vertical swimming behavior the vertical structure of the velocity field can be of critical importance in simulating trajectories and estimating final connectivity patterns [*Paris and Cowen*, 2004].

[14] Open boundaries were chosen over periodic north and south boundaries in order to include the effects of remotely driven circulation. *Gan and Allen* [2005] demonstrated the effect of open boundary conditions (OBC), using a radiation condition, on cases involving the propagation of coastally trapped waves (CTW). When winds were relatively uniform in the alongshore direction, they found that results with OBC were similar to those with periodic boundary conditions. However, in cases with spatially variable wind fields, disturbances within the domain or originating at the southern boundary (CTW propagation direction is northward on the California coast) were able to propagate through and

out of the domain when using OBC. This effect is particularly important in the region of this study where stronger winds to the south may provide a significant proportion of the forcing for local circulation. *Pringle and Riser* [2003] explored this possibility in the temperature records of an upwelling region off San Diego (Pt. Loma) and found that temperature fluctuations were correlated with winds off Baja California hundreds of km to the south, with a lag time consistent with CTW [*Lentz and Winant*, 1986]. Forcing from outside the domain is also important in this region because of the presence of topographic features such as seamounts and submarine canyons, which have a strong influence on the surrounding circulation.

[15] The open boundary conditions in the model employ a radiation scheme with separate algorithms for the inward and outward fluxes, plus adaptive nudging to the external data, described by *Marchesiello et al.* [2001]. Data for the inner domain OBC are generated by one-way nesting within the larger domain model run with closed boundaries. We

believe that the closed boundaries are sufficiently distant from the area of interest that the effect is small over the limited time of the simulations, while still retaining information from wind forcing off Baja California.

[16] Additional tests were conducted using different wind forcing products (or no forcing) on the inner and outer domains to assess the relative influence of remote versus local wind forcing. The forcing through boundary conditions from the outer domain affected the circulation in differing degrees depending on the wind product used. Satellite wind forcing, which had the lowest resolution and largest mean wind speeds, was applied to both inner and outer domains in one test, and to only the outer domain in another, with very similar results. However, when a higher-resolution modeled wind field was used, with weaker and more variable wind speeds, a significant difference in the circulation was observed depending upon whether it was applied to only the outer domain, or applied to both inner and outer domains. More detailed analysis of wind forcing issues follows.

3. Model Forcing Comparisons

[17] The availability of accurate wind field data at sufficiently high resolution continues to be a problem for the forcing of small-scale models. The most accurate products to date include QuikSCAT satellite scatterometer wind data, and mesoscale atmospheric models such as COAMPS (Coupled Ocean/Atmosphere Mesoscale Prediction System) and RSM (Regional Spectral Model). *Di Lorenzo* [2003] compared the effects of monthly averages of several wind products on a ROMS simulation of the southern California Current, and concluded that RSM produced the most accurate streamlines and velocity fields. However the RSM model grid size is larger than desired for inner shelf processes, and for transport on those scales, climatological averages are too coarse to resolve events which can occur over time periods of hours to days.

[18] However small-scale variability within 20 km of shore remains unresolved. RSM downscaled winds have a 10 km spatial resolution. At best they may only partially capture the high spatial variability of wind fields in the 20–30 km closest to shore where much of the transport from point source pollutants, kelp forests, or rocky reef habitats occurs. QuikSCAT winds are resolved only to the resolution of the scatterometer footprint (25 × 37 km) and land falling within that range interferes with the signal. Post-processing methods that eliminate low-velocity data can improve the accuracy of nearshore QuikSCAT data [*Pickett et al.*, 2003], but this can be problematic in regions where nearshore winds are characterized by high variability and low velocity (see below). Algorithms for estimating and reducing the effects of land contamination have produced reasonable data much closer to shore however the proximity to shore within which data can be retrieved is greater with higher wind speeds [*Owen et al.*, 2007]. A blended product is promising in that it could take advantage of the distances offshore where each product is most accurate. *Chao et al.* [2003] compared QuikSCAT satellite winds and modeled COAMPS winds with in situ data from three coastal buoys ranging from 20–100 km offshore, and developed a blended product from the two which outperformed either individual product. However

one has yet to be developed utilizing fine-scale data near the shoreline required for near shore transport processes. Wind forcing from the NCAR/Penn State Fifth Generation Mesoscale Model (MM5) at scales of several kilometers have recently become available also. MM5 in intercomparison studies has performed similarly to RSM at comparable resolutions [*Gutzler et al.*, 2004] and nested products have shown further improvements.

[19] Resolving small-scale wind variability is particularly important in regions with strong topographic effects. The present domain, in the lee of Pt Conception, is also frequently in the wind shadow of Dana Point and the southern Channel Islands. The wind field and Ekman layer depth in this region is similar to that directly leeward of Catalina Island (where the Catalina Eddy develops in the wind field) where a pronounced wind shadow appears to be responsible for reduced surface mixing and warmer ocean surface temperatures [*Caldiera and Marchesiello*, 2002]. Modeled mesoscale wind fields frequently capture cross-shelf variability on scales of order 10 km, and are therefore more likely to create cross-shelf shear, eddies, and other small-scale features in the model than satellite winds. The diurnal cycle is captured reasonably well in the 10 km California reanalysis downscaling of RSM winds (CaRD10) [*Kanamitsu and Kanamaru*, 2007]. The correlation and root mean square error between the RSM winds and buoy observations near shore within the Cataline Eddy were significantly better than for NCEP/NCAR reanalysis winds in the same location, although the wind speed was slightly larger in the modeled winds. The RSM wind speed at the shoreline is also slightly higher than data collected at the Scripps Pier, by a factor of 1.4 for u and 1.3 for v. In addition, RSM winds at the shoreline are not highly correlated with actual hourly wind measurements taken at Scripps Pier ($r_u = 0.41$ and $r_v = 0.10$, Figure 3). The difference might be especially important when simulating processes such as dispersion and transport of larvae spawning at the shoreline, or recruitment events. Because of this, we tested how nearshore flow fields are affected by forcing the inner domain with directly measured shoreline wind data, while using model or satellite forcing on the outer domain.

[20] In the small-scale simulations of the San Diego coastline we tested three wind products with temporal resolution of 1–6 hours, comparing velocity fields and distribution patterns of passive tracers to determine how sensitive final results are to the choice of wind forcing. Choice of wind products was further limited by the geographical extent of some of the models (e.g., MM5 does not extend south of the U.S./Mexico border.) The tests included forcing from hourly winds measured at Scripps Pier meteorological station applied uniformly over the inner and/or outer domain (SIO forcing), a 6 hr blend of NCEP reanalysis and QuikSCAT scatterometer wind fields (QKS forcing), and hourly Regional Spectral Model 10 km resolution CaRD10 data (RSM forcing). Tests were run with different combinations of forcing on the inner and outer domains. Because of the inherent problems with nearshore wind accuracy in both the modeled and scatterometer products, all three were tested on the outer domains while using SIO forcing on the inner domain (SIO/SIO, QKS/SIO and RSM/SIO). A test was also conducted in which the higher-resolution RSM winds, which
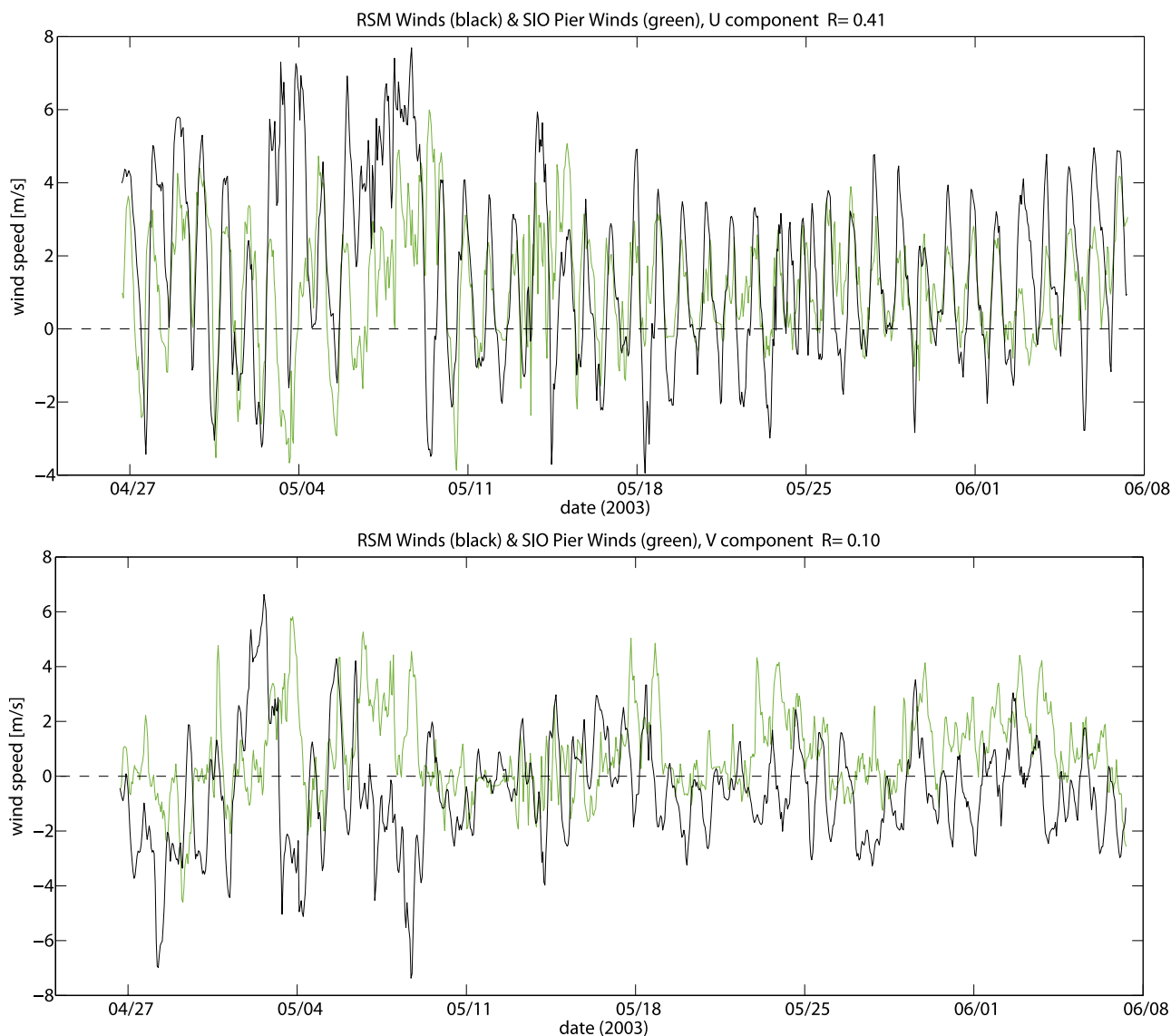
Figure 3. Comparison of RSM 10-m wind speed at Scripps Pier location and in situ measurements from Scripps Pier for May 2003. Top: u component (E−W, positive westward), Bottom: v component (N−S, positive northward). RSM winds in black, Pier winds in green. Correlation coefficients are 0.41 for u, 0.10 for v.

extend closer to shore than QuikSCAT, were applied to the both the inner and outer domains (RSM/RSM). Because of the low spatial and temporal resolution of the satellite winds, and the 30-km land contamination zone, these were considered to be poorly suited for the inner model. Runs were also conducted with SIO forcing on the outer domain and no forcing on the inner domain to use as a minimal-forcing reference point (SIO/None).

[21] Scripps Pier (SIO) winds were obtained from the Coastal Data Information Program (CDIP) at Scripps Institution of Oceanography. The wind stress drag coefficient was computed according to *Yelland and Taylor* [1996] and is nearly the same as the estimate given by *Large and Pond* [1981] for lower wind speeds. The mean surface wind stress calculated in RSM at the Scripps Pier coordinate was higher than the SIO wind stress by a factor of 10, and a pattern of

anomalously high wind stress is seen in several other places near shore in the RSM data.

3.1. Comparison of Velocity Fields

[22] Major differences in the velocity fields were observed between the various forcing combinations, particularly in the flow magnitude and variance (Figure 4). The higher-resolution RSM winds, when applied to both the inner and outer domains, produce the greatest velocities and variances. To help ascertain which forcing combination most closely approximated actual conditions, the models were compared to in situ current data from the region. Because no instruments were deployed in the area during May 2003, when larval fingerprinting field experiments were conducted, model results for May 2003 were compared to data available from May 2006 from an ADCP deployment during April–July 2006 in the San Diego–La Jolla Ecological Reserve
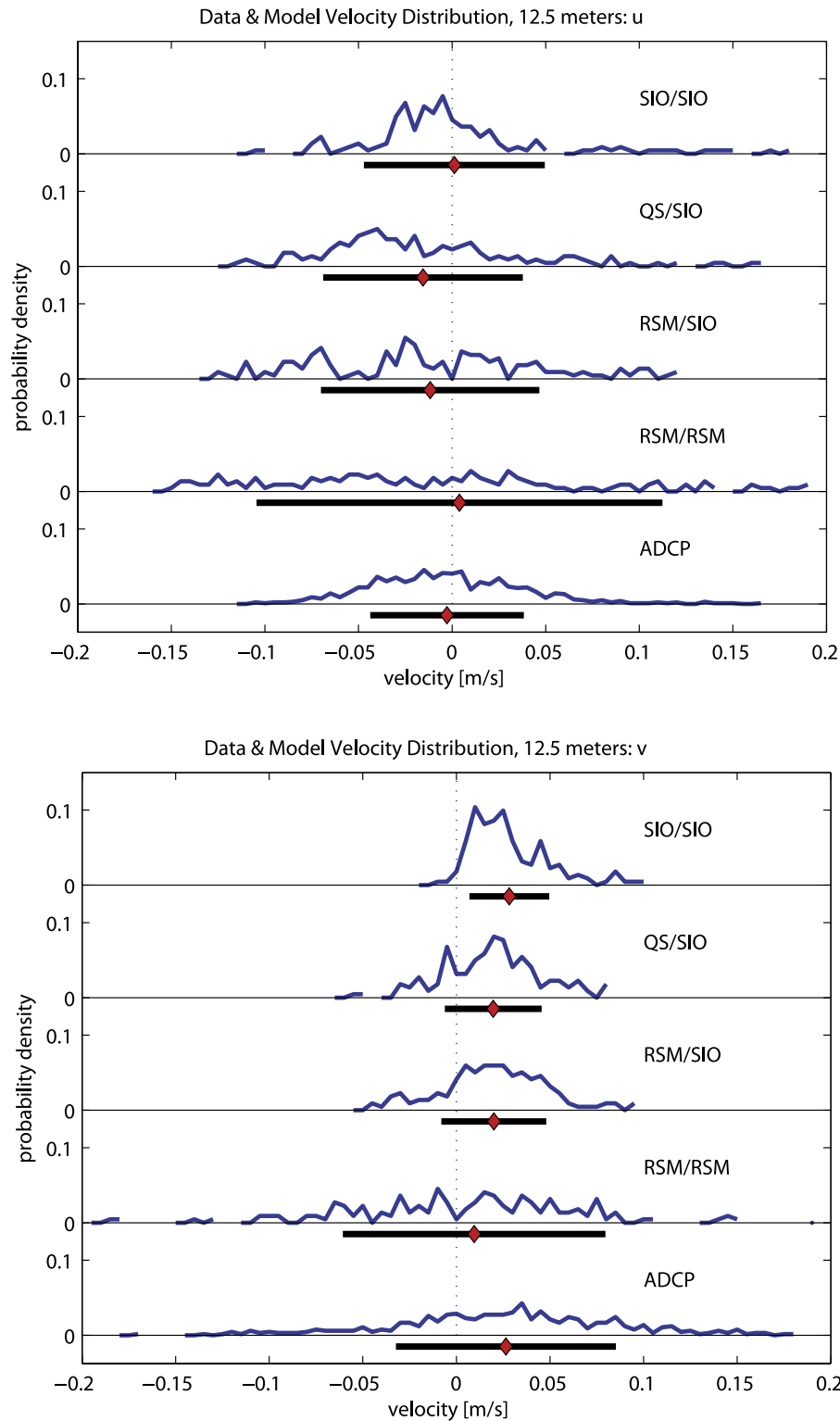
Figure 4. Probability density distribution, mean, and standard deviation for u (eastward, cross-shore) and v (northward, alongshore) for ADCP data and simulations over one month. Measured velocity is from 12.5 m below surface, at a bottom depth of 33 m for May 2006. Model velocity is taken from the grid cell corresponding to the instrument location in simulations run for May 2003. Red markers indicate the mean, and the black lines are ±1 standard deviations.

(near larval release site 5, Figure 1). RSM 10-km wind forcing is not currently available for 2006 for model–data comparisons. The time series of current directions are not expected to match however the variance in the magnitude of the u and v components should be roughly comparable since conditions during the two years were similar (no El Niño/La

Table 1. P-values From Analysis of Variance for ADCP Data Versus ROMS Simulations[a]

	SIO/SIO	QKS/SIO	RSM/SIO	RSM/RSM
		u		
sfc	<0.01	<0.01	<0.01	<0.01
3 m	0.27	0.01	0.04	**0.64**
10 m	0.86	0.01	0.04	**0.98**
20 m	0.05	0.38	0.33	**0.92**
30 m	0.58	**1.00**	0.90	<0.01
		v		
sfc	<0.01	<0.01	<0.01	<0.01
3 m	0.03	0.09	0.09	**0.92**
10 m	**0.69**	0.40	0.39	0.10
20 m	0.19	0.13	**0.26**	<0.01
30 m	**0.85**	<0.01	<0.01	<0.01
mean	0.35	0.20	0.21	**0.36**

[a]One-way ANOVA analyses were performed for discrete depths, comparing ADCP cross-shore (*u*) and alongshore velocity (*v*) to each individual model for a 3-week time series at 6 hr intervals (N = 165). ADCP data are from a 33 m upward-looking instrument deployed during May 2006. Model data are from the corresponding grid cell location. Columns indicate the forcing combination used for the outer domain (providing boundary conditions) and the inner domain (boundary/inner) for May 2003 simulations. Highest P-values for each depth are shown in bold.

Niña, no large storms, predominantly northward winds). The ADCP data were filtered to remove tidal effects (typically a few cm s^{-1} in magnitude). The model data were taken from the grid cell corresponding to the instrument location, with bottom depth of 33 m off La Jolla. A comparison depth of 12.5 m was chosen because ADCP data and model velocities for all forcing combinations are most similar at mid-depths, away from the effects of top and bottom boundaries. The probability density distributions, means, and variance of the alongshore velocity, *v* are most similar between the ADCP data and the RSM/RSM forcing combination (Figure 4). However cross-shore ADCP velocity has a stronger correspondence with the RSM-SIO model.

[23] Analysis of variance was also performed to assess the similarity between the model and ADCP velocities at discrete depths over the 3-week model runs. The P-value is a measure of the difference between data sets, typically a set of observations and a set of predicted values. P is the probability that the observed between-group variability (ADCP vs model) would occur by chance if the two groups of data were related (i.e., if the mean and variance of the ADCP data were well-represented by the model). In general, P-values are highest in the upper water column for the RSM−RSM forcing combination, while in the lower water column the highest P-values occur in simulations run with SIO forcing on the inner domain (Table 1). Differences in surface variance is captured the poorest. The mean P-values averaged over all depths are highest and nearly identical for the SIO/SIO case (0.32) and for the RSM/RSM case (0.31). However the trends in the two are opposite, with SIO/SIO wind forcing performing better in the lower water column while RSM/RSM wind forcing performs better in the upper water column (surface excluded).

3.2. Comparison of Vertical Structure

[24] In simulations of larval dispersion and connectivity, the vertical structure of velocity often strongly influences trajectories. Surface velocities are typically strongest, and

direction and speed may change with depth. The effects of vertically variable currents on passive larvae are predictable if vertical mixing is properly represented, but vertical behavior of larvae can influence transport pathways and final larval supply to recruitment regions. Thus capturing vertical variability in the water column can be critical for determining patterns of connectivity if larvae migrate vertically during their planktonic period or exhibit ontogenetically shifting photo- or geotaxis.

[25] The field ADCP measurements also show that near-surface currents are often opposed to near-bottom currents. As a test of model performance, observed (2006 data) and model simulations (2003 output) are compared in terms of the fraction of time that current velocities are opposed to those near-bottom. This comparison is calculated for a variety of depths and shown in Table 2 (top). While near-surface ADCP velocities are opposed to near-bottom velocities 46% of the time, this is less common for model results. A maximum of 42% is obtained for the RSM/RSM model run, but this opposing flow is less likely in other model runs (22−36%). Measures of vertical shear irrespective of flow direction also indicate a better performance of the RSM/RSM model compared to the other forcing combinations (Table 2, center). The root mean square (RMS) difference between near bottom currents and currents at 20, 10, 3, and 1 meters depth increases from 0.04 cm s^{-1} to 0.37 cm s^{-1} in the ADCP data, and the range for the RSM/RSM model is 0.09−0.16 cm s^{-1}. In the other model runs the range is only 0.3−0.5 cm s^{-1}. When viewed by layer, the RSM/RSM configuration fairly closely approximates the measured vertical shear in all but the surface layer, where a strong shear is present in the ADCP data between 1−3 meters depth (Table 2, bottom).

[26] This difference suggests that while the RSM/RSM model is more accurately representing the effects of surface

Table 2. Comparison of Vertical Velocity Structure[a]

Forcing Combination	SIO/SIO	QKS/SIO	RSM/SIO	RSM/RSM	ADCP
Currents Oppose Bottom (% time)					
1 m below sfc	0.34	0.19	0.23	0.47	0.46
3 m below sfc	0.33	0.18	0.22	0.47	0.46
10 m below sfc	0.25	0.24	0.21	0.42	0.34
20 m below sfc	0.29	0.15	0.13	0.16	0.19
Vertical Shear From Bottom (RMS)					
1 m below sfc-bottom	0.04	0.04	0.05	0.12	0.37
3 m below sfc-bottom	0.04	0.04	0.04	0.11	0.16
10 m below sfc-bottom	0.03	0.04	0.04	0.08	0.08
20 m below sfc-bottom	0.03	0.03	0.04	0.06	0.04
Vertical Shear by Layer (RMS)					
1−3 m below sfc	0.01	0.01	0.01	0.01	0.26
3−10 m below sfc	0.03	0.03	0.03	0.07	0.15
10−20 m below sfc	0.02	0.03	0.04	0.05	0.07
20−30 m below sfc	0.03	0.03	0.04	0.06	0.04

[a](top) Fraction of time alongshore currents at depths of 1, 3, 10 and 20 meters below the surface are in the opposite direction from bottom currents (32 m depth) for different forcing combinations and ADCP data. Center: Root mean square differnce between bottom currents (m s^{-1}) and currents at depths of 1, 3, 10 and 20 meters below the surface. (bottom) RMS difference in currents between individual layers. Location is near site 4 (La Jolla) at a water column depth of 33 m (see Figure 1 for site locations). Data are shown for an upward looking ADCP deployed during May 2006. Model data are from the corresponding grid cell location. Columns indicate the forcing combination used for the outer domain (providing boundary conditions) and the inner domain (i.e., boundary/inner) for May 2003 simulations.
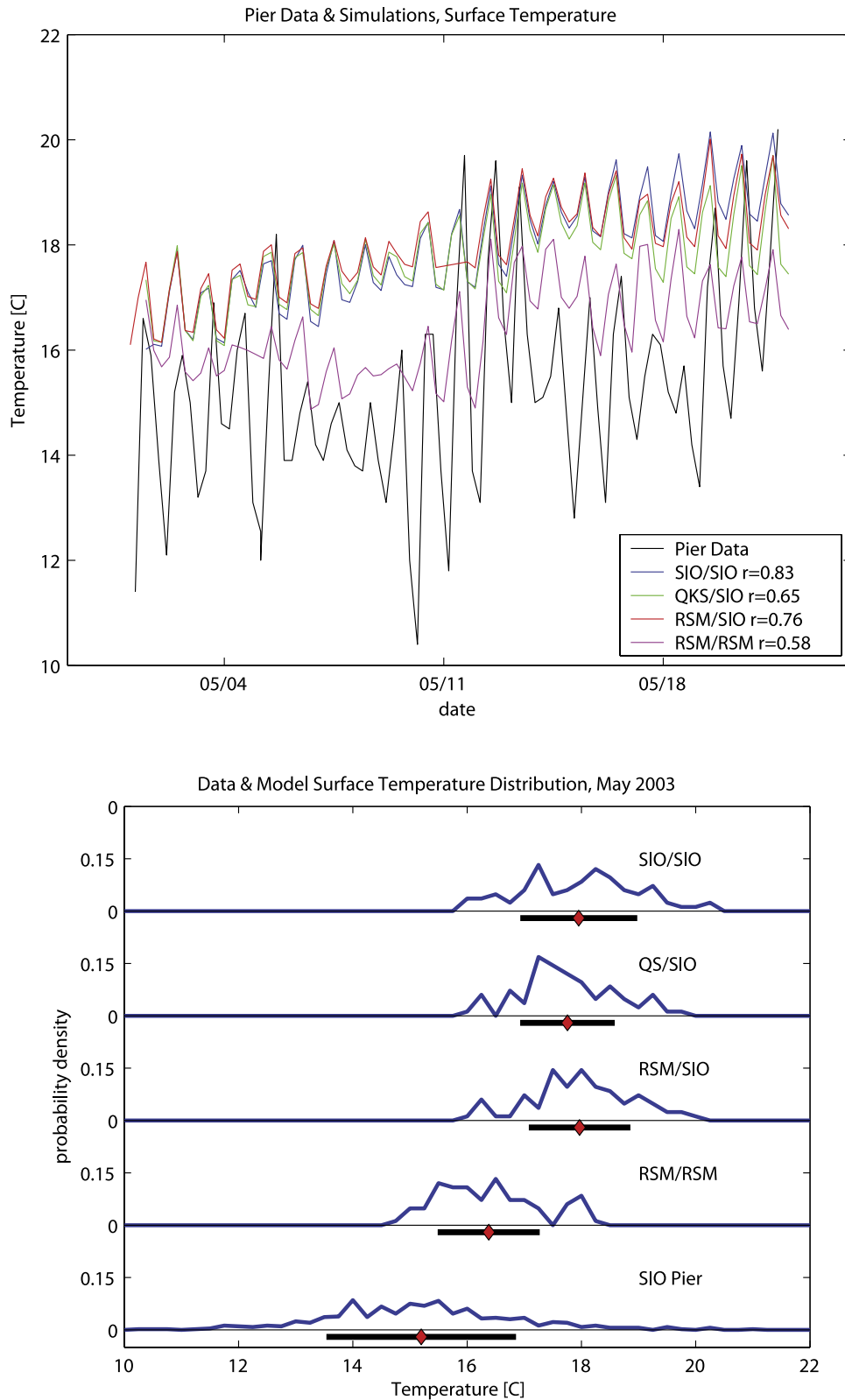
Figure 5. Comparison of temperature from Scripps Pier shore stations data and ROMS simulations. (top) Temperature times series for May 2003. Upper series are simulations with no forcing on the inner domain, or Scripps Pier wind forcing applied uniformly over the domain. The lower series are the pier data, and the simulation run with RSM forcing on both the outer domain (providing boundary conditions) and inner domain. (bottom) Probability density distribution of surface temperatures from models and Shore Stations pier data for May 2003. Red marker indicates the mean, and black line is ±1 standard deviation.

Table 3. Comparison of May 2003 Surface Temperature Data From Scrips Pier (Shore Stations Program) and ROMS Simulations With Different Combinations of Forcing on the Outer/Inner Domains[a]

Simulation	Mean T [°C]	r	F-value	P-value
Pier data	15.2	–	–	–
SIO/none	18.1	0.65	143.1	0.00
SIO/SIO	18.0	0.81	125.8	0.00
QKS/SIO	17.6	0.60	116.8	0.00
RSM/SIO	17.8	0.73	117.5	0.00
RSM/RSM	15.6	0.70	2.4	0.12

[a]One-way ANOVA analyses were performed to compare in situ temperature data against each individual model for a 1 month time series at 6 hr intervals. Model surface temperatures are taken from the upper grid cell location containing the pier coordinates.

wind stress and stratification, which typically account for mid-water and near-surface shear, the surface shear is still underestimated. This is seen with all wind forcing combinations and may have origins in the limited resolution of the short-wave forcing which does not capture the high variability of energy creating surface stratification, or in the limitations of the turbulent vertical mixing scheme in the model.

3.3. Comparison of Model Temperatures

[27] Very few temperature time series are available during this period (2003–2006) with which to compare model results. However hourly temperature records exist for the Scripps Pier from the extensive Shore Stations time series (http://shorestation.ucsd.edu). Comparing the pier surface temperature to that in the corresponding model grid cell for the same time period, May 2003, we see different results depending upon the combinations of wind forcing used in the simulations (Figure 5). All simulations had correlations (r) between 0.65 and 0.83 with the pier temperature data. However the model run with uniform Scripps pier wind forcing over the outer domain (to provide boundary conditions) and no wind or heat flux forcing in the inner domain (SIO/none) shows primarily a regular diurnal cycle of temperature in a range slightly higher than that of the pier data. Other combinations that were run with SIO winds and climatic heat flux forcing for the inner domain, and a variety of forcing products tested on the outer domain, also closely follow the diurnal periodicity as well as the temperature range. The highest correlation is with the SIO/SIO simulation however the range is biased toward temperatures higher than the pier data in all the simulations using SIO forcing on the inner domain. The only combination that approximates the mean and probability density distribution of the Scripps pier data is the simulation run with RSM wind forcing on both the inner and outer domains (Figure 5 bottom, Table 3). The RSM/RSM model shows a greater correspondence with the Scripps pier data in one-way ANOVA analysis as well. Although the correlation for the ADCP data and the RSM/RSM model is in the middle of the range of r values for the model comparisons, the F-values (measure of between-group variability) and P-values (probability that the between-group variability could occur by chance in data sets drawn from the same group) depart significantly from the other models (Table 3). Between-group variability is much smaller ($F = 2.4$ compared to 117–143) and the probability of this occurring in two samples drawn from the same data is

much larger (0.12 compared to <0.001). While this is still not a high correspondence, by this measure the RSM/RSM case performs better.

3.4. Comparison of Dispersion Patterns

[28] The effects of differences in model fields on transport and dispersion larval tracers originating at the shoreline can be seen in maps of tracer concentrations (Figures 6 and 7). For these experiments passive tracers were released at 9 sites arranged north to south along the shore corresponding to known *Mytilus californianus* mussel populations (see site locations in Figure 1). The same sites are used as tracer collection points after a specified time, chosen to approximate the period larvae would likely develop in the water column before recruitment onto a suitable substrate (planktonic larval duration, PLD). The original tracer concentration is $10^7/m^3$. Dispersion patterns for three combinations of forcing are compared: SIO/QuikSCAT, RSM/RSM, and RSM/SIO (indicating the outer model forcing used to create the open boundary conditions, and the inner model forcing, respectively).

[29] Depending on the forcing used, there are variations in the distance and direction of tracer advection and the degree of dispersion. The advection distance of tracer originating from site 5 is significantly less when the outer domain is forced with RSM wind than when forced with QuikSCAT winds (Figure 6, left and center columns). This may be the result of the wind field downscaled from the lower resolution (25 km) QuikSCAT product, which does not include scatterometer data within 30 km of shore where winds are weakest. The resulting tracer field after a 14-day planktonic larval duration is a northward surface plume in all three cases (Figure 8, upper row). However the tracer concentration along the shoreline and the extent of offshore mixing is significantly different depending on the forcing used.

[30] Differing results between wind forcing products are even more evident in the tracer released from site 9, where small-scale topographic effects are particularly important. This site is located in the lee south of Pt. Loma, near the mouth of San Diego Bay, where there is a local retention zone and frequent spring-summer upwelling [*Roughan et al.*, 2005]. The initial flow in the QuikSCAT/SIO simulation is to the north, which advects tracer into the lee of the point where it is partially retained (Figure 7, left column). However the initial RSM wind forcing drives flow briefly to the south. When used only for the outer domain to provide boundary conditions, the result is a southward plume which hugs the coast, then reverses direction and flows back into the lee of the point (Figure 7, center column). When the RSM forcing is applied to both the inner and outer domains, the southward flow is much stronger and by day 5 nearly all tracer has advected out of the domain (Figure 7, right column). The final tracer concentrations after 14 days are strikingly different depending on the forcing combination used (Figure 8, bottom row). The variation ranges from high concentrations along most of the coastline north of site 9, as well as in plumes offshore (QuikSCAT/SIO); to high concentrations south of site 9 and for a limited distance north, in a plume hugging the shoreline (RSM/SIO), to tracer almost entirely absent from the entire inner domain (RSM/RSM).

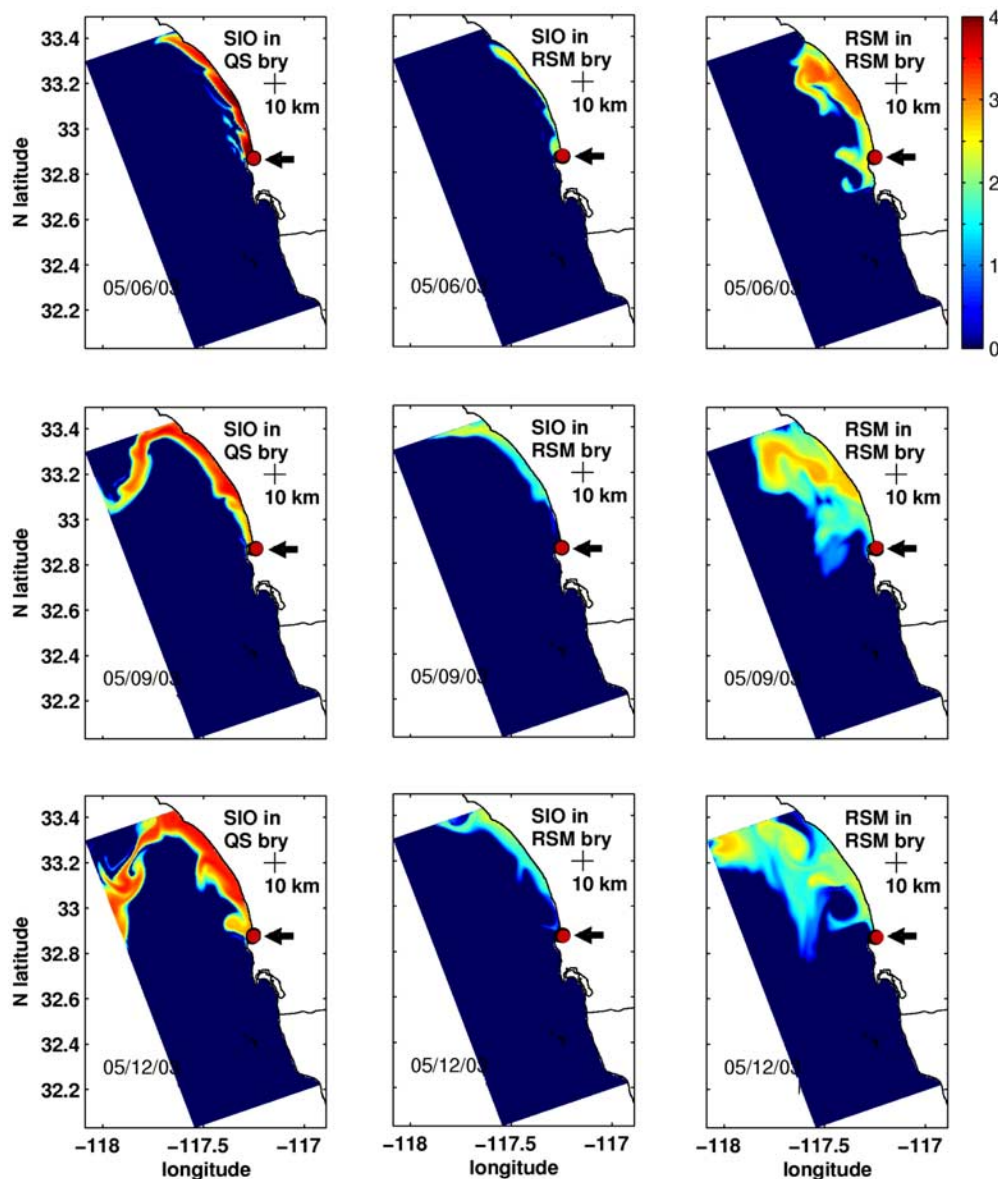**Figure 6.** Time series of tracer distributions at the surface, 5, 8, and 11 days after release from site 5 (initial concentration $10^7/m^3$). Three forcing combinations are shown: QuikSCAT/NCEP reanalysis forcing on the outer domain, SIO Pier winds on the inner domain (left column); Regional Spectral Model 10 km downscaled winds (RSM) on both inner and outer domains (center column); and RSM winds on the outer domain with Scripps Pier winds on the inner domain (right column). Simulations of the outer domain are used for open boundary conditions on the inner domain which is shown in the figures. Release site is indicated by red dot.

[31] While predominantly northward flow is evident in all three cases, the pattern as well as the extent of alongshore and offshore transport of the tracer differs significantly among runs with different forcing. The three forcing combinations also respond differently to topographic effects, such as the embayment south of Pt. Loma at the mouth of San Diego Bay. As a result, at some release sites, while there may be variations in final tracer concentrations, the advective pathways may be similar. At release sites within the range of influence of more prominent topographic features, the advective pathways may be entirely different

depending on the forcing product used. Even small differences in wind forcing can be amplified by interaction with topography and appear as major differences in dispersion. The tendency for different forcing products to produce different advection pathways and dispersion patterns is not well recognized, although this has significant consequences for estimates of larval transport and population connectivity.

3.5. Applications to Larval Connectivity

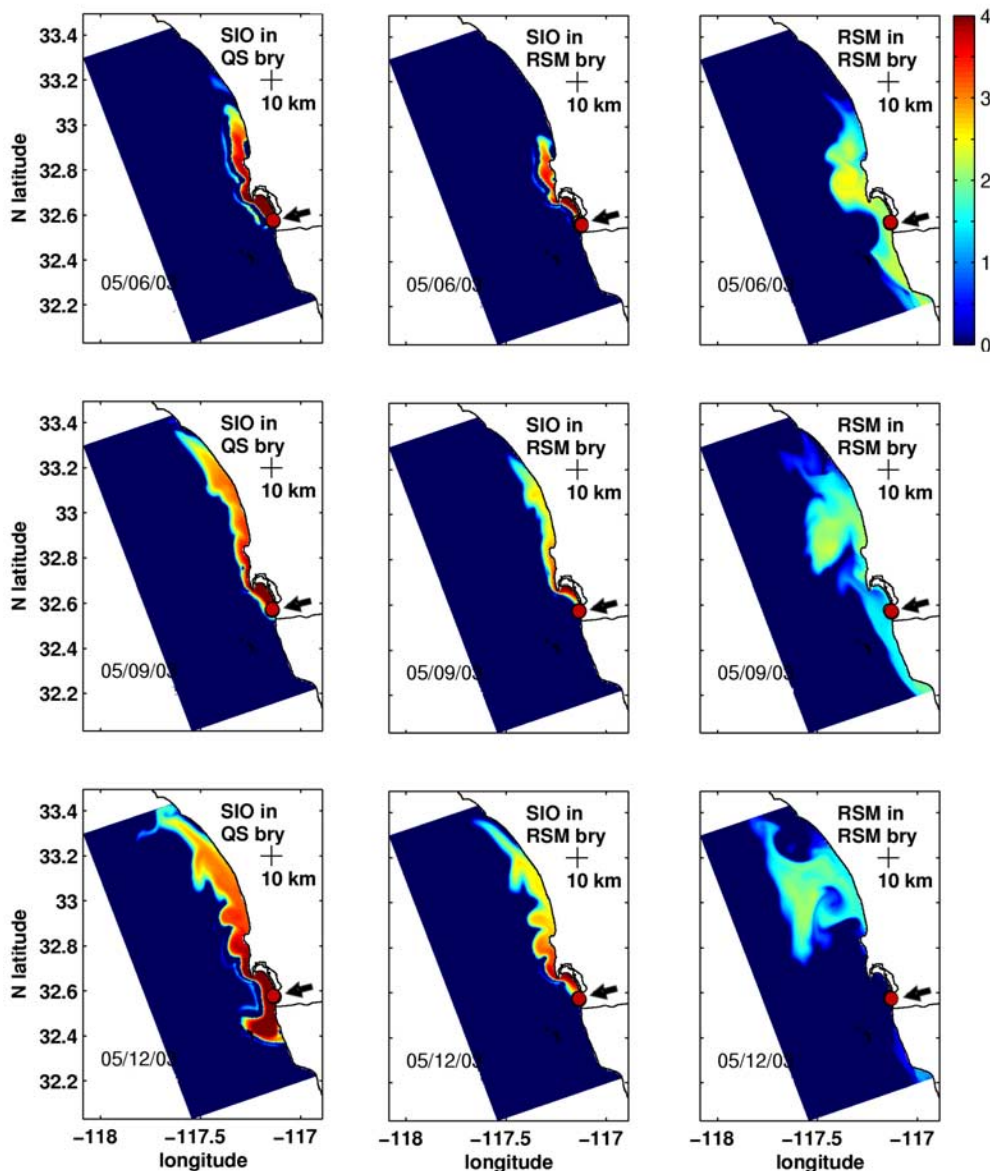[32] Simulations of physical circulation such as those presented above are commonly used to estimate connectiv-

Figure 7. Time series of tracer distributions at the surface, 5, 8 and 11 days after release from site 9 (initial concentration $10^7/m^3$). Three forcing combinations are shown: QuikSCAT/NCEP reanalysis forcing on the outer domain, SIO Pier winds on the inner domain (left column); regional Spectral Model 10 km downscaled winds (RSM) on both inner and outer domains (center column); and RSM winds on the outer domain with Scripps Pier winds on the inner domain (right column). Simulations of the outer domain are used for open boundary conditions on the inner domain which is shown in the figures. Release site is indicated by red dot.

ity of populations that disperse via planktonic larvae [*Cowen et al.*, 2000; *James et al.*, 2002; *Paris et al.*, 2005; *Mitarai et al.*, 2007]. The results shown here demonstrate how the outcome of such an experiment could be quite different depending on which forcing product is used. Typical measures of population connectivity include estimates of tracer sources and destinations, the importance of self-seeding to the sustainability of individual populations, the relative contribution of individual populations to larval export, and the absolute magnitudes of potential larval

recruitment by populations [*James et al.*, 2002; *Hastings and Botsford*, 2006; *Levin*, 2006; *Cowen et al.*, 2007].

[33] The effects of model uncertainty on the estimation of relative tracer distribution and source composition at each simulated larval collection site is illustrated in Figure 9 for the three final model forcing configurations (QKS/SIO, RSM/SIO, and RSM/RSM). Connectivities can be represented by tabulating the concentration of tracer at each collection site that has originated at each release site. The collection date is set to correspond to a species' planktonic
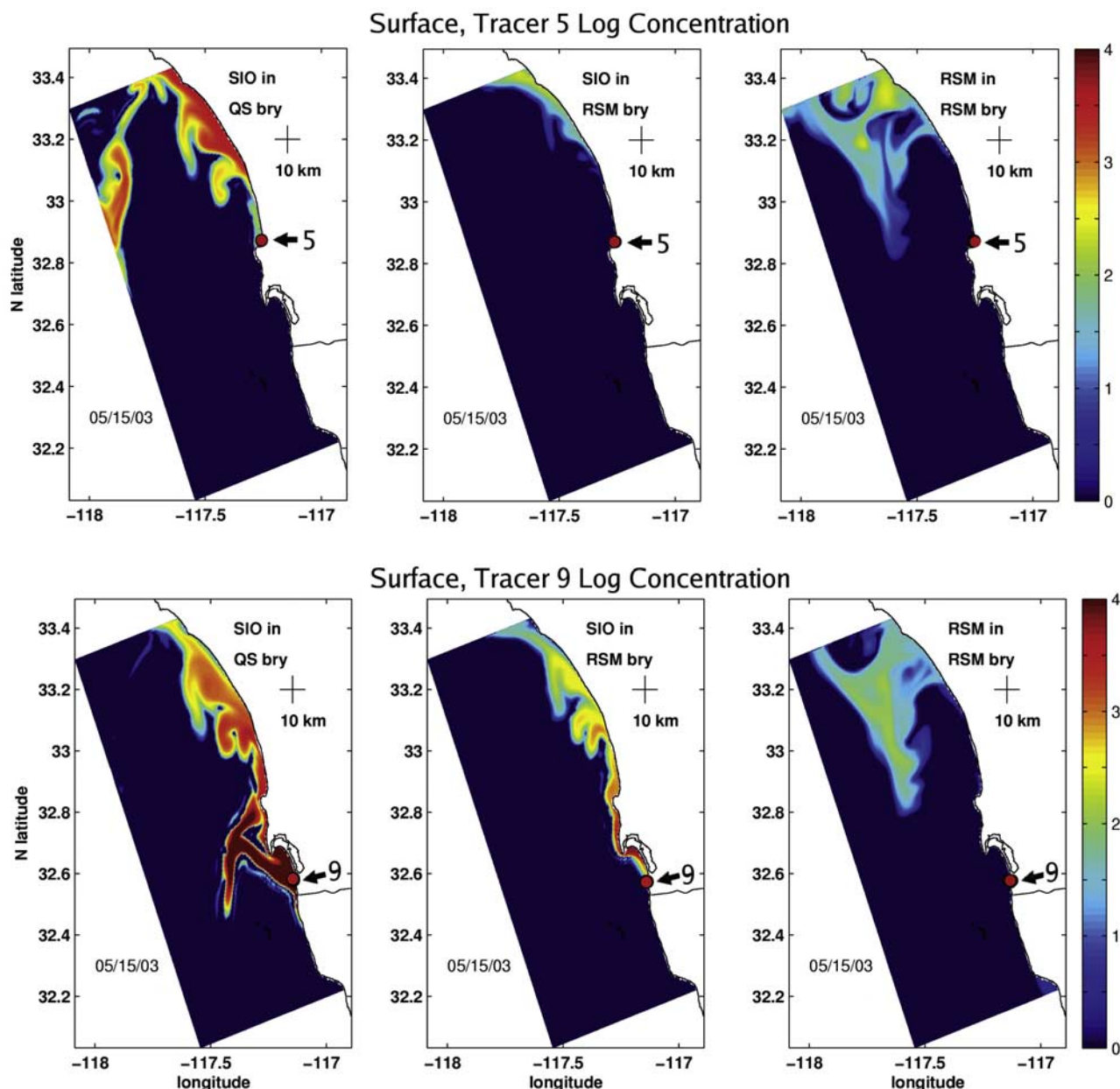
Figure 8. Tracer distributions at the surface at the end of a 14-day larval planktonic duration for three forcing combinations: QuikSCAT/NCEP reanalysis on the outer domain, Scripps Pier winds on the inner domain (QS/SIO, left); Regional Spectral Model 10 km downscaled winds (RSM) winds on the outer domain with SCripps Pier winds on the inner domain (RSM/SIO, center); and RSM winds on both inner and outer domains (RSM/RSM, right). Simulations of the outer domain are used for open boundary conditions on the inner domain which is shown in the figures. Top panels show tracer released from site 5 and bottom panels show tracer released from site 9 to the south. Release sites are indicated by red dots. Tracer is shown in units of log concentration 14 days after release (initial concentration $10^7/m^3$).

larval duration, in this case 14 days. The predominant direction of dispersal is similar for all three cases with sites near the leading edge of the northward flowing larval plume receiving more potential larvae. However the origin of tracer collected at each site is significantly different. The collection sites in the QKS/SIO model have an approximately equal contribution from all tracer origination sites except the northernmost ones, which have advected out of the domain, while the final distribution in the RSM/SIO model is dominated by the three southernmost sites. With differing circulation magnitude and a lack of retention south of Pt. Loma, the RSM/RSM model has lost all the tracer from that area (site 9) to southward advection, while tracer from sites 7 and 8 just north of the point still dominate the composition at the other sites.

[34] Differences in the percentage of self-seeding (larvae settling at the same site where they were released), export, and import are also evident. Sites which could be inter-
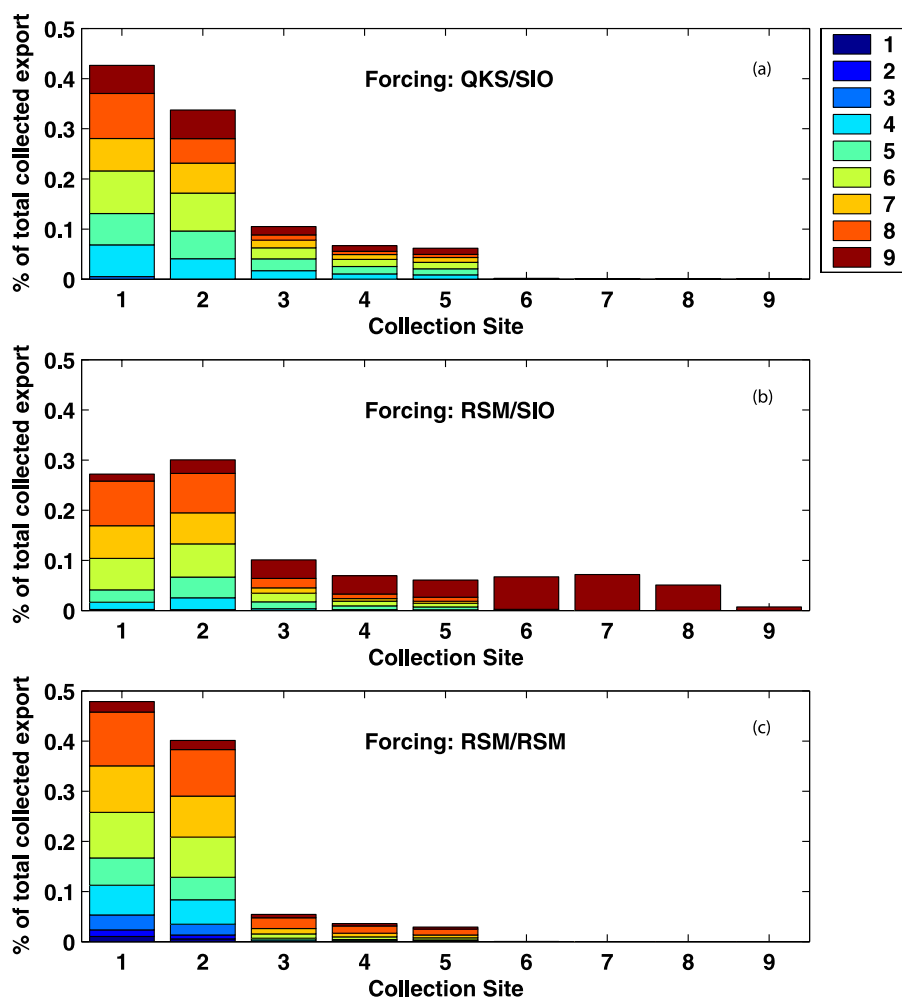
Figure 9. Origin of tracer collected at each simulated larval release/recruitment site 14 days after release for three forcing combinations. (a) QKS/SIO, QuikSCAT forcing on boundaries, Scripps Pier wind forcing on inner domain; (b) RSM/SIO, RSM forcing on boundaries, Scripps pier winds on inner domain; and (c) RSM/RSM, RSM forcing on boundaries and inner domain. Bars heights show relative amount of tracer collected at each site, and colors indicate the tracer source (site 1 blue–site 9 red; see Figure 1 for site locations). Tracer concentrations are normalized by the total amount of all tracer collected at all sites.

preted as predominantly self-seeding vary depending on the forcing used (Figure 10a), as do sites which would be considered important exporters (sources) of larvae to the system (Figure 10b). Another consequence of choice of forcing which is likely to be overlooked without comparing products is the total "number" of larvae that arrive at settlement sites (Figure 10c). The absolute number of larvae arriving at a settlement site will affect how robust the recruitment event is, for example, whether or not a new population of recruits will be substantially compromised by an event causing a high degree of mortality. Thus the relative importance of an export source must be put in context with the absolute amount it contributes to other sites. For example, the total tracer captured at settlement sites in the RSM/RSM case is 2–5 orders of magnitude lower than in simulations run with other forcing. So although sites 6 and 7 appear to be major exporters in the RSM/RSM case (Figure 10b), the total tracer they export to

other sites is much lower than lesser exporters in the other two cases (Figure 10c). Simulations using a statistical approach involving continuous releases and cumulative analysis of tracer pathways over longer time scales will only compound the potential model error, not clarify it, if each time step is similarly subject to forcing inaccuracies. When combined with the natural intermittency and variability of the system, which models capture only partially, the uncertainties introduced by forcing will be difficult to distinguish and quantify.

4. Discussion

[35] The continental shelf is one of the most biologically productive zones in the coastal ocean because of terrestrial nutrient inputs, wind-driven upwelling, and frontal dynamics [*Falkowski et al.*, 1994; *Csanady*, 1990; *Eppley and Peterson*, 1979]. It is also one of the most complex in terms
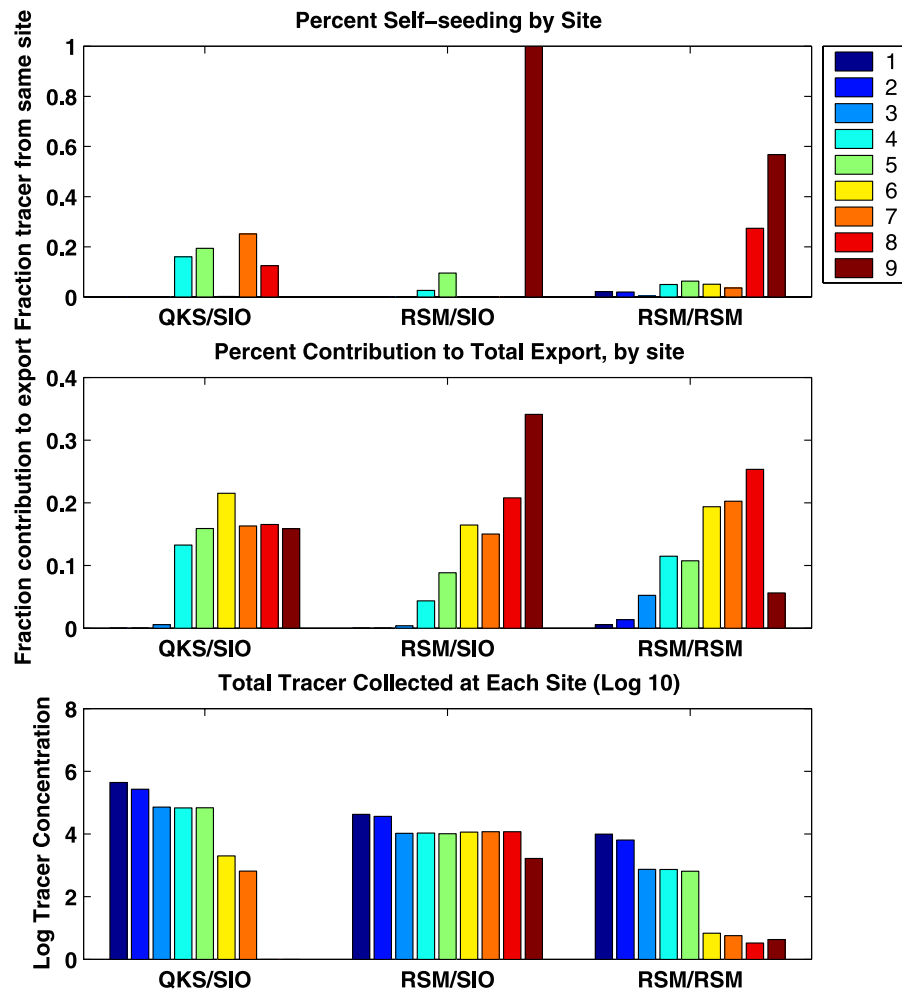
Figure 10. Comparison of forcing combinations: impact on processes relevant to larval connectivity. Forcing shown is QKS/SIO,QuikSCAT forcing on boundaries, Scripps Pier wind forcing on inner domain; RSM/SIO, RSM forcing on boundaries, Scripps Pier winds on inner domain; and RSM/RSM, RSM forcing on boundaries and inner domain. Sites 1–9 are along coast, north to south (see Figure 1). Top: Self-seeding percentage. Fraction of tracer measured at each site which originated at the same site. Center: Percent contribution of each site to total export among all sites. Only tracer that is collected at potential settlement sites (i.e., sites 1–9) is included. Bottom: total tracer collected from each site, units in log-10 of tracer concentration measured in a column of one grid cell area, over all depths.

of small-scale temporal and spatial variability of the physical fields. With its diversity of habitats, from rocky reefs and kelp forests, to subtidal sands and steep submarine canyons, it is a critically important zone to understand in order to assess the viability of marine reserves for long term protection of coastal populations. A small-scale regional model can provide a practical means of conducting experiments to investigate dispersion problems, including passive pollutants or active biological transport involving multiple parameters such as larval planktonic duration, release time, fecundity, mortality and swimming behavior.

[36] For models to be useful in such experiments however the input parameters and forcing must be sufficient to simulate the processes that are important. Recent discourse on the challenges of interdisciplinary marine studies and modeling have pointed out that in coastal areas such processes can have very short temporal and spatial scales,

irregular distributions, episodic occurrences, non-linear dynamics, and may have feedback to and from multiple scales [*Lermusiaux*, 2006; *Robinson et al.*, 1999]. *Siegel et al.* [2008] have shown that even under idealized conditions, with alongshore uniformity of both wind and bathymetry, larval dispersal and connectivity patterns were irregular over scales of tens of kilometers and subject to significant episodic forcing events. Because wind is the primary physical driver of many coastal systems, lack of resolution or uncertainties in wind forcing can have important consequences. If combined with small-scale irregularities in topography, these consequences would be magnified further.

[37] Other studies have detailed effects of the uncertainties in wind speed and wind stress curl that increase with proximity to the shoreline. *Capet et al.* [2004] observed that in the COAMPS models, alongshore wind speed drop-off occurred at different distances from shore, ranging from 10 to

50 km, depending on the resolution of the meteorological model. COAMPS nearshore wind speeds were lower than buoy measurements and the resulting wind stress curl was more pronounced, causing a bias toward upwelling processes because of Ekman pumping over Ekman transport. Similarly *Marchesiello et al.* [2003] noted the offshore distance of the zero-wind-curl line varied from 150 km in their 0.5° wind model (COADS), to 300 km in the 1° models (COADS and NCEP). In their 20 km resolution ROMS simulation comparisons there was a relationship between the depth of the coastal undercurrent and the coastal wind stress curl which was particularly pronounced in the 150 km closest to shore. Similar uncertainty is present in the RSM nearshore wind fields where wind speed and the calculated wind stress is significantly higher than observations.

[38] The uncertainty in wind forcing affects model results and connectivity estimates, as illustrated by comparisons of tracer origin at simulated collection sites. Self-seeding and relative export of larvae, two other measures important for determining the sustainability of populations, also differ significantly, as does the absolute number of larvae arriving at potential recruitment sites. Erroneously high (or low) offshore transport away from spawning sites influences the number of larvae available to local populations as well. Alongshore velocities and the scale of eddies increase with distance from shore thus relatively small error in the degree of cross-shore transport can lead to significant uncertainty in estimates of alongshore transport and mixing [*Gawarkiewicz et al.*, 2007; *Largier*, 2003].

[39] This study highlights the importance of developing "non-sterilized simulations" with realistic forcing and topography, including estimates of uncertainty [*Karniadakis and Glimm*, 2006]. However one of the major challenges in applying numerical ocean models to applications in ecology and environmental science is that not only are wind forcing and dispersion patterns naturally variable and episodic, the uncertainty associated with model input is difficult to quantify. This calls for new tools including more sophisticated statistical approaches as well as incorporation of data from developing ocean observing systems [*Lermusiaux*, 2006]. Additional coastal observations are also clearly needed to help ground-truth modeled nearshore winds and resolve the uncertainties in model forcing. Resolution of ocean and atmospheric observations nearshore, particularly cross-shelf and near topographic features, will be especially critical in providing a means to validate model results.

[40] At present the most robust approaches for estimating population connectivity appear to be those which combine both physical modeling and field experiments. Because both approaches have distinct limitations, collaboration provides a necessary system of reality checks on results. Field limitations include the impracticality of tracking larvae in the field on the scales required for connectivity studies (tens to hundreds of kilometers) due to their very small size and high rate of dilution, mixing, and mortality during transport. Filtering seawater for larvae is complicated by the problem of determining the species of larvae when there are two or more indistinguishable species cohabiting the area. Several indirect methods show promise for determining dispersion and connectivity patterns. Among these are the use of genetic markers and microchemical "fingerprinting" of

Table A1. Input Parameters for San Diego ROMS Simulations

Parameter	Value	Units
Time step (dt)	75	sec
Horizontal tracer diffusion coefficient (tnu2), salt	5.0	m²/s
Horizontal tracer diffusion coefficient (tnu2), heat	1.5	m²/s
Horizontal viscosity coefficient (visc2)	5.0	m²/s
Background vertical mixing coefficients	5×10^{-6}	m²/s
Boundary nudging/relaxation time scale, tracers	4	dy
Boundary nudging/relaxation time scale, zeta	1	dy
Boundary nudging/relaxation time scale, momentum	4	dy
Linear bottom drag coefficient	8×10^{-7}	m/s
Mean density	1025	kg/m³
Passive/active OBC factor	5	
Thermal expansion coefficient	−0.1	
Saline contraction coefficient	0.0	

larvae that produce carbonate structures such as shells, otoliths and statoliths while in their planktonic period [*Thorrold et al.*, 2002; *Arkhipkin et al.*, 2004; *Levin*, 2006; *Thorrold et al.*, 2007; *Hedgecock et al.*, 2007]. Methods based on genetic differences between populations are suitable to investigate processes with evolutionary time scales and basin-scale domains, or to populations which have low connectivity. However elemental fingerprinting is useful for investigating single events, seasonal or interannual variability in connectivity which occur on timescales of weeks to months. Thus it is a good match for the short time scales of small-scale or regional models.

[41] The models can then provide a method of experimentation that is unavailable in the field, while field data provide important constraints on model parameters, initialization and assessment of results. Model results in turn inform decisions about experimental design and interpretation of collected data. Together this collaborative approach serves to stimulate questions and improvements in both approaches, and brings to light data needs essential for resolving connectivity processes that operate on regional scales. One of the most pressing of these data needs is for higher-resolution measurement of coastal wind fields, for which there is presently little available to ground-truth wind forcing products in this critical area.

Appendix A: Input Parameters

[42] Table A1.

References

Anderson, D., B. Keafer, W. R. Geyer, R. P. Signell, and T. C. Loder (2005), Toxic Alexandrium blooms in the western Gulf of Maine: The plume advection hypothesis revisited, *Limnol. Oceanogr.*, *50*(1), 328–345.

Arkhipkin, A., S. E. Campana, J. FitzGerald, and S. R. Thorrold (2004), Spatial and temporal variation in elemental signatures of statoliths from the Patagonian longfin squid (*Loligo gahi*), *Can. J. Fish. Aquat. Sci.*, *61*(7), 1212–1224, doi:10.1139/f04-075.

Becker, B. J., L. A. Levin, F. J. Fodrie, and P. McMillan (2007), Complex larval connectivity patterns among marine invertebrate populations, *Proc. Natl. Acad. Sci.*, *104*(9), 3267–3272.

Beckmann, A., and D. Haidvogel (1993), Numerical simulation of flow around a tall isolated seamount: Part I: Problem formulation and model accuracy, *J. Phys. Oceanogr.*, *23*, 1736–1753.

Byers, J. E., and J. M. Pringle (2006), Going against the flow: Retention, range limits and invasions in advective environments, *Mar. Ecol. Prog. Ser.*, *313*, 27–41.

Caldiera, R. M. A., and P. Marchesiello (2002), Ocean response to wind sheltering in the Southern California Bight, *Geophys. Res. Lett.*, *29*(13), 1635, doi:10.1029/2001GL014563.

Caldeira, R. M. A., P. Marchesiello, N. P. Nezlin, P. M. DiGiacomo, and J. C. McWilliams (2005), Island wakes in the Southern California Bight, *J. Geophys. Res.*, *110*, C11012, doi:10.1029/2004JC002675.

Capet, X. J., P. Marchesiello, and J. C. McWilliams (2004), Upwelling response to coastal wind profiles, *Geophys. Res. Lett.*, *31*, L13311, doi:10.1029/2004GL020123.

Cervantes, B. T. K., and J. S. Allen (2006), Numerical model simulations of continental shelf flows off northern California, *Deep Sea Res.*, *53*(25–26), 2956.

Chao, Y., Z. Li, J. Kindle, J. Paduan, and F. Chavez (2003), A high-resolution surface vector wind product for coastal oceans: Blending satellite scatterometer measurements with regional mesoscale atmospheric model simulations, *Geophys. Res. Lett.*, *30*(1), 1013, doi:10.1029/2002GL015729.

Cowen, R. K., K. M. Lwiza, S. Sponaugle, C. B. Paris, and D. B. Olson (2000), Connectivity of marine populations: Open or closed?, *Science*, *287*, 857–859.

Cowen, R. K., G. Gawarkiewicz, J. Pineda, S. Thorrold, and F. Werner (2007), Population connectivity in marine systems: An overview, *Oceanography*, *20*(3), 14–21.

Csanady, G. T. (1990), Physical basis of coastal productivity, The SEEP and MASAR experiments, *Eos. Trans. AGU*, *71*(36), 1060–1065.

Di Lorenzo, E. (2003), Seasonal dynamics of the surface circulation in the Southern California Current System, *Deep Sea Res. II*, *50*(14–16), 2371–2388.

Di Lorenzo, E., A. J. Miller, N. Schneider, and J. McWilliams (2005), The warming of the California current system: Dynamics and ecosystem implications, *J. Phys. Oceanogr.*, *35*(3), 336–362.

Dong, C., and J. C. McWilliams (2007), A numerical study of island wakes in the Southern California Bight, *Cont. Shelf Res.*, *27*, 1233–1248.

Eppley, R. W., and B. J. Peterson (1979), Particulate organic matter flux and planktonic new production in the deep ocean, *Nature*, *282*, 670–680.

Falkowski, P., P. Biscaye, and C. Sancetta (1994), The lateral flux of bioenic particles from the eastern North American continental margin to the North Atlantic Ocean, *Deep Sea Res. II*, *41*(2/3), 583–601.

Galindo, H. M., D. B. Olson, and S. R. Palumbi (2006), Seascape genetics: A coupled oceanographic-genetic model predicts population structure of Caribbean corals, *Curr. Biol.*, *16*, 1622–1626.

Gan, J., and J. Allen (2005), On open boundary conditions for a limited-area coastal model off Oregon. part 1: Response to idealized wind forcing, *Ocean Modell.*, *8*(1–2), 115–133.

Gawarkiewicz, G., S. Monismith, and J. Largier (2007), Observing larval transport processes affecting population connectivity, *Oceanography*, *20*(3), 40–53.

Gutzler, D., et al. (2004), The North American Monsoon Model Assessment Project (NAMAP), NCEP/Climate Prediction Center Atlas 11, 32 pp. (Available at http://www.cpc.ncep.noaa.gov/research_papers/ncep_cpc_atlas/11/atlas11.htm)

Haney, R. L. (1991), On the pressure gradient force over steep topography in sigma coordinate ocean models, *J. Phys. Oceanogr.*, *22*, 892–902.

Hastings, A., and L. Botsford (2006), Persistence of spatial populations depends on returning home, *Proc. Natl. Acad. Sci.*, *103*(17), 6067–6072.

Hedgecock, D., P. H. Barber, and S. Edmands (2007), Genetic approaches to measuring connectivity, *Oceanography*, *20*(3), 70–79.

Hodgins, D. O., S. W. Tinis, and L. A. Taylor (1998), Marine sewage outfall assessment for the capital regional district, British Columbia, using nested three-dimensional models, *Water Sci. Technol.*, *38*(10), 301–308.

James, M. K., P. R. Armsworth, L. B. Mason, and L. Bode (2002), The structure of reef fish metapopulations: Modeling larval dispersal and retention patterns, *Proc. Biol. Sci.*, *269*, 2079–2086.

Johnson, D. R., H. M. Perry, and W. M. Graham (2005), Using nowcast model currents to explore transport of non-indigenous jellyfish into the Gulf of Mexico, *Mar. Ecol. Prog. Ser.*, *305*.

Kanamitsu, M., and H. Kanamaru (2007), 57-year California reanalysis downscaling at 10 km (CaRD10). part 1: System detail and validation with observations, *J. Clim.*, *20*, 5553–5571.

Karniadakis, G., and J. Glimm (2006), Uncertainty estimation and prediction for interdisciplinary ocean dynamics, *J. Comput. Phys.*, *217*, 1–4.

Kettle, A. J., and K. Haines (2006), How does the European eel (*Anguilla anguilla*) retain its population structure during its larval migration across the North Atlantic Ocean?, *Can. J. Fish. Aquat. Sci.*, *63*(1), 90–106.

Kinlan, B. P., and S. D. Gaines (2003), Propagule dispersal in marine and terrestrial environments: A community perspective, *Ecology*, *84*(8), 2007–2020.

Koné, V., E. Machu, P. Penven, V. Andersen, V. Garcon, P. Fréon, and H. Demarcq (2005), Modeling the primary and secondary productions of the southern Benguela upwelling system: A comparative study through two biogeochemical models, *Global Biogeochem. Cycles*, *19*, GB4021, doi:10.1029/2004GB002427.

Large, W. G., and S. Pond (1981), Open ocean momentum flux measurements in moderate to strong winds, *J. Phys. Oceanogr.*, *11*, 324–336.

Large, W. G., J. C. McWilliams, and S. C. Doney (1994), Oceanic vertical mixing: A review and a model with nonlocal boundary layer parameterization, *Rev. Geophys.*, *32*(4), 363–403.

Largier, J. L. (2003), Considerations in estimating larval dispersal distances from oceanographic data, *Ecol. Appl.*, *13*, S71–S89.

Lentz, S., and C. Winant (1986), Subinertial Currents on the Southern California Shelf, *J. Phys. Oceanogr.*, *16*(11), 1737–1750.

Lermusiaux, P. (2006), Uncertainty estimation and prediction for interdisciplinary ocean dynamics, *J. Comput. Phys.*, *217*, 176–199.

Levin, L. A. (2006), Recent progress in understanding larval dispersal: New directions and digressions, *Integr. Comp. Biol.*, *46*(3), 282–297.

Marchesiello, P., J. C. McWilliams, and A. Shchepetkin (2001), Open boundary conditions for long-term integration of regional oceanic models, *Ocean Modell.*, *3*(1), 20.

Marchesiello, P., J. McWilliams, and A. Shchepetkin (2003), Equilibrium structure and dynamics of the California current system, *J. Phys. Oceanogr.*, *33*(4), 753–783.

Mellor, G. L., L.-Y. Oey, and T. Ezer (1998), Sigma coordinate pressure gradient errors and the seamount problem, *J. Atmos. Oceanic Technol.*, *15*(5), 1122–1131.

Mitarai, S., D. Siegel, and K. Winters (2007), A numerical study of stochastic larval settlement in the California Current system, *J. Mar. Syst.*, doi:10.1016/j.jmarsys.2006.02.017.

Moore, A. M., H. G. Arango, E. D. Lorenzo, B. D. Cornuelle, A. J. Miller, and D. J. Neilson (2004), A comprehensive ocean prediction and analysis system based on the tangent linear and adjoint of a regional ocean model, *Ocean Modell.*, *7*(1–2), 227–258.

Owen, M. P., K. M. Stuart, and D. G. Long (2007), Ultra-high-resolution near-coastal wind retrieval for QuikSCAT, *Proc. SPIE (Coast. Ocean Remote Sens.)*, *6680*, doi:10.1117/12.732681.

Palumbi, S. R. (2003), Population genetics, demographic connectivity, and the design of marine reserves, *Ecol. Appl.*, *13*, S146–S158.

Paris, C., and R. K. Cowen (2004), Direct evidence of a biophysical retention mechanism for coral reef fish larvae, *Limnol. Oceanogr.*, *49*(6), 1964–1979.

Paris, C. B., R. K. Cowen, R. Claro, and K. C. Lindeman (2005), Larval transport pathways from Cuban spawning aggregations (Snappers; Lutjanidae) based on biophysical modeling, *Mar. Ecol. Prog. Ser.*, *296*, 93–106.

Penven, P., L. Debreua, P. Marchesiello, and J. C. McWilliams (2006), Evaluation and application of the ROMS 1-way embedding procedure to the central California upwelling system, *Ocean Modell.*, *12*(1–2), 157–187.

Pickett, M. H., W. Tang, L. K. Rosenfeld, and C. H. Wash (2003), QuikSCAT Satellite Comparisons with Nearshore Buoy Wind Data off the U.S. West Coast, *J. Atmos. Oceanic Technol.*, *20*(12), 1869–1879.

Pringle, J., and K. Riser (2003), Remotely forced nearshore upwelling in Southern California, *J. Geophys. Res.*, *108*(C4), 3131, doi:10.1029/2002JC001447.

Robinson, A. R., J. J. McCarthy, and B. J. Rothschild (1999), Interdisciplinary ocean science is evolving and a systems approach is essential, *J. Mar. Syst.*, *22*, 231–239.

Roughan, M., E. J. Terril, J. L. Largier, and M. P. Otero (2005), Observations of divergence and upwelling around Point Loma, *J. Geophys. Res.*, *110*, C04011, doi:10.1029/2004JC002662.

Scotti, A., and J. Pineda (2007), Plankton accumulation and transport in propagating nonlinear internal fronts, *J. Mar. Res.*, *65*, 117–145.

Shchepetkin, A., and J. McWilliams (2005), The regional oceanic modeling system (ROMS): A split-explicit, free-surface, topography-following-coordinate oceanic model, *Ocean Modell.*, *9*(4), 347–404.

She, J., and J. M. Klinck (2000), Flow near submarine canyons driven by constant upwelling winds, *J. Geophys. Res.*, *105*(28), 28,671–28,694.

Siegel, D. A., B. P. Kinlan, B. Gaylord, and S. D. Gaines (2003), Lagrangian descriptions of marine larval dispersion, *Mar. Ecol. Prog. Ser.*, *260*, 83–96.

Siegel, D. A., S. Mitarai, C. J. Costello, S. D. Gaines, B. E. Kendall, R. R. Warner, and K. B. Winters (2008), The stochastic nature of larval connectivity among nearshore marine populations, *Proc. Natl. Acad. Sci.*, *105*(26), 8974–8979.

Signell, R. P., and W. R. Geyer (1991), Transient eddy formation around headlands, *J. Geophys. Res.*, *96*(C2), 2561–2575.

Signell, R., H. Jenter, and A. Blumberg (2000), Predicting the physical effects of relocating Boston's sewage outfall, *J. Estuarine Coastal Shelf Sci.*, *50*, 59–72.

Song, Y., and D. Haidvogel (1994), A semi-implicit ocean circulation model using a generalized topography-following coordinate system, *J. Comput. Phys.*, *115*(1), 228–244.

Thorrold, S. R., G. P. Jones, M. E. Hellberg, R. S. Burton, S. E. Swearer, J. E. Niegel, S. G. Morgan, and R. R. Warner (2002), Quantifying larval retention and connectivity in marine populations with artificial and natural markers, *Bull. Mar. Sci.*, *70*(1), 291–308, suppl.

Thorrold, S. R., D. C. Zacherl, and L. A. Levin (2007), Population connectivity and larval dispersal: Using geochemical signatures in calcified structures, *Oceanography*, *20*(3), 80–89.

Warner, J. C., W. R. Geyer, and J. A. Lerczak (2005), Numerical modeling of an estuary: A comprehensive skill assessment, *J. Geophys. Res.*, *110*, C05001, doi:10.1029/2004JC002691.

Washburn, L., B. H. Jones, A. Bratkovich, T. D. Dickey, and M.-S. Chen (1992), Mixing, dispersion, and resuspension in vicinity of ocean wastewater plume, *J. Hydraul. Eng.*, *118*(1), 38–58.

Werner, F., R. Cowen, and C. Paris (2007), Coupled biological and physical models, *Oceanography*, *20*(3), 54–69.

Yelland, M., and P. K. Taylor (1996), Wind stress measurements from the Open Ocean, *J. Phys. Oceanogr.*, *26*, 541–558.

————————

B. D. Cornuelle, Physical Oceanography Research Division, Scripps Institution of Oceanography, 9500 Gilman Drive, Mail Code 0230, La Jolla, CA 92037-0230, USA.

E. Di Lorenzo, School of Earth and Atmospheric Sciences, Georgia Institute of Technology, 311 Ferst Drive, Atlanta, GA 30332-0340, USA.

J. L. Largier, Bodega Marine Laboratory, University of California, P.O. Box 247, Davis, CA 94923, USA.

L. A. Levin and L. L. Rasmussen, Division of Integrative Oceanography, Scripps Institution of Oceanography, 9500 Gilman Drive, Mail Code 0218, La Jolla, CA 92037-0218, USA. (raz@ucsd.edu)